Role of tensor meson pole and Δ exchange diagrams in $p\bar{p}\to\pi^+\pi^-$

Y. Yan and R. Tegen
Department of Physics, University of the Witwatersrand, P.O. WITS, Johannesburg 2050, South Africa
(Received 20 May 1996)

The $\bar{N}N\to\pi\pi$ annihilation reaction is investigated in a model with both baryon-exchange diagrams and meson-pole diagrams. The main features of the observed differential cross sections for $p\bar{p}\to\pi^+\pi^-$ from 360 to 1190 MeV/c are well understood in this model. The backward enhancement of the differential cross section is mainly due to the $N\Delta\pi$ tensor coupling while the process $p\bar{p}\to f_2\to\pi^+\pi^-$ contributes to the bump structure around 100° developing for $P_{\rm lab}>680$ MeV/c. This hints at nontrivial quark spin contributions beyond the $^3P_0$ model (which favored S and P waves) and hints at a large gluonic component in tensor mesons with masses between 1.27 and 2.2 GeV. [S0556-2813(96)04109-X]

PACS number(s): 13.75.Cs, 14.20.Dh, 21.30.Cb, 24.85.+p

I. INTRODUCTION

The recent production of a handful of antihydrogen atoms at LEAR [1] has refocused theoretical interest on the understanding of the interaction between matter and antimatter within quantum chromodynamics (QCD). Most data on matter-antimatter interactions have been collected for the low-energy $p\bar{p}$ system [2] with some early data from CERN at higher energies (momenta in the range from 0.9 to 2.4 GeV/c [3]). The existence of antimatter is a natural consequence of the Dirac equation describing the fermionic constituents of all hadrons, the quarks and antiquarks, and their interactions with the gluons. One would like to explain the $p\bar{p}$ interaction, as one example, in terms of the underlying quark-gluon dynamics of QCD. The complexity of relativistic quark-gluon dynamics necessitates more detailed experimental information than branching ratios for the different annihilation channels. Differential cross sections for various energies have so far been measured only for the two-body channels $p\bar{p}\to p\bar{p}$ (elastic, EL), $n\bar{n}$ (charge-exchange, CEX), $\pi^+\pi^-$, and K^+K^-. Having experimental information on the angular and energy dependence of the reaction $p\bar{p}\to\pi^+\pi^-$ has turned out to be crucial for the unraveling of the two dominant features of this reaction; see below. Unlike the NN interaction, which is the main ingredient of any microscopic description of nuclear physics, the (EL) and (CEX) reactions in the NN regime have an imaginary component due to the annihilation. The real component can be related via a G-parity transformation [4,5] to the NN interaction. The meson-exchange part (OBEP) of the NN and $N\bar{N}$ interactions is the same for G-even meson exchanges (for example, ρ and σ) and opposite in sign for G-odd meson exchanges (for example, ω), so that in particular the short-ranged ω exchange is repulsive in NN whereas it is strongly attractive in the $N\bar{N}$ system. In order to account for the nonobservation of narrow $N\bar{N}$ resonances (baryonium) a relatively small annihilation strength (imaginary component of the $N\bar{N}$ interaction) is sufficient [6]. This imaginary component of the $N\bar{N}$ interaction can be built at the hadronic level from all annihilation channels [7] $N\bar{N}\to M_1M_2, M_1M_2M_3, M_1\cdots$ ($M_i=$ meson). It is observed that on the average $n=5\pm1$ pions are produced [2,3]. Many channels can in fact be simulated by quasi-two-body reactions, for example, $N\bar{N}\to\rho\rho$ with $\rho\to\pi\pi$. It is, therefore, imperative to understand first the reactions $N\bar{N}\to M_1M_2$ before one can try to ''tackle'' more complex channels (i.e., more than two mesons in the final state). The understanding of the $N\bar{N}$ annihilation at the quark-gluon level is still in its infancies. In an optical potential approach, a quark-gluon annihilation potential for $N\bar{N}\to N\bar{N}$ (EL and CEX) has been derived [8]. Its range is r dependent and corresponds to a relativistic quark-antiquark overlap for a relative distance r of the N and $\bar{N}$ centers. This state- and energy-independent annihilation potential describes data well between 390 MeV/c and 860 MeV/c [9,10]. The model, however, fails to explain the annihilation strength due to a lack of reliable information on gluonium states. It has turned out that experimental data on angular dependences of cross sections at various energies from close to threshold, $P_{\rm lab}=0$ and $E_{\rm c.m.}=1876$ MeV, to $P_{\rm lab}$ around 1 GeV/c are crucial for the understanding of the underlying QCD dynamics. This is the case for the reactions $p\bar{p}\to M_1M_2$ with $M_{1,2}=\pi^\pm$ and $K^\pm$. Here we concentrate on the simplest reaction $p\bar{p}\to\pi^+\pi^-$ for which very detailed data are available [3,11,12]. The real part of the T matrix for this reaction is described by baryon exchange (N,Δ,N^*,Δ^*) with half off-shell vertex functions and baryon propagators originating in the underlying QCD dynamics. Usually only N and Δ are taken into account; for other nucleon resonances, vertex functions are less well known. The imaginary part of this reaction probes the resonant content of the $N\bar{N}$ and $\pi\pi$ systems. The C-, P-, and G-parity operations lead to selection rules

$$G(N\bar{N})=(-1)^{L+S+I_{N\bar{N}}}, \tag{1}$$

$$G(\pi\pi)=(-1)^{L'+I_{\pi\pi}}=+1, \tag{2}$$

where L (L') refers to the $N\bar{N}$ ($\pi\pi$) system and S is the total spin of the $N\bar{N}$ system. Parity conservation leads to $L'=L\pm1$ which allows only certain combinations of $^{2S+1}L_J$ for the $N\bar{N}$ system, $^3P_{0,2}, ^3F_{2,4}, ^3H_{4,6},\ldots$ for $(P,C,I)=(+,+,0)$ and $L'=$ even, and $^3S_1, ^3D_{1,3}, ^3G_{3,5},\ldots$ for $(P,C,I)=(-,-,1)$ and $L'=$ odd

 © 1996 The American Physical Society

[4,5]. Only G-even $p\bar{p}$ states can be probed by investigating the $\pi\pi$ final states. The inclusion of $p\bar{p}\to K^+K^-$ would allow us to probe also G-odd $p\bar{p}$ states. In this paper we concentrate on the $\pi\pi$ final state and leave KK and other two-particle final states for another occasion.

We find that an important contribution to $p\bar{p}\to\pi\pi$ is the G-even tensor mesons f_2 in the range 1270−2150 MeV [13]; their contribution is shown here to lead to the observed bump structure around 100° developing for momenta 680 MeV/c and above (visible already in the old CERN data [3] between 0.9 GeV/c and 1.23 GeV/c). The importance of total angular momenta $J\leqslant 3$ has recently been pointed out by Kloet and Myhrer [14]. They find from their amplitude analysis of $p\bar{p}\to\pi^+\pi^-$ that very few partial waves are needed (i.e., the interaction is much shorter ranged than the OPEP-dominated EL reaction which requires many more partial waves), with $J=2$ contributions being important at lower momenta while $J=3$ contributions becoming important beyond 500 MeV/c. This indicates to us that at higher momenta the contributions of spin-3 mesons, $\rho_3(1690)$, and spin-4 mesons, $f_4(2050)$, might have to be included for a more detailed fit of the data. It is interesting to note that the final state interaction (FSI) via a $\rho\rho$ intermediate state can also produce a bump around 100° [15]. As a side remark we mention that most of the f_2 resonances decay into $\pi\pi$ and $K\bar{K}$. Although the branching ratio[1] for the $\pi\pi$ final state is less than 1% this angular dependence (a dip-bump structure) is also present in the elastic (EL) reaction $p\bar{p}\to p\bar{p}$ in the same momentum range [8–10]. The bump structure is also observed in K^+K^- and could have the same origin (the flavor-blind gluonium states would, apart from phase space arguments, decay equally into $\pi\pi$ and $K\bar{K}$); however, the G-odd ''partners'' of the f_2 meson, the $a_2(1320)$ and $\pi_2(1670)$ [13], could also contribute to $K\bar{K}$, and indeed they do [13]. This suggests that there must be a connection between the f_2 meson-pole diagram and the

$$p\bar{p}\to\left\{\begin{array}{c} GGG \\ GGq\bar{q} \\ Gq^2\bar{q}^2 \end{array}\right\}\to\left\{\begin{array}{c} \pi\pi \\ K\bar{K} \end{array}\right\} \tag{3}$$

quark-gluon annihilation diagrams. This strong correlation (with the quantum numbers of the f_2) among the GGG, $GGq\bar{q}$, and $Gq^2\bar{q}^2$ intermediate states is presently missing in any of the quark-gluon models. This ''hint'' from an analysis of the hadronic diagrams could help to better model the propagation of the above-mentioned gluonic intermediate states. Much work has already been done in this direction [16]. Because of the complexity of nonperturbative QCD in this reaction $(3q+3\bar{q}\to 2q+2\bar{q})$, there is, however, room for improvement. Hadronic models can help to identify the problem areas at the quark-gluon level.

Apart from the bump structure around 100°, which is visible in both $\pi^+\pi^-$ and K^+K^- beyond 680 MeV/c, there is another striking feature of these reactions which current quark-gluon models of the annihilation have problems with. The differential cross sections for both $\pi^+\pi^-$ and K^+K^- channels show a distinct rise towards backward angles. In our baryon-exchange plus meson resonance model of the annihilation we show that this ''backward rise'' can be attributed to the tensor strength of the $\pi N\Delta$ vertex function. This effect was first made visible in the work of Moussallam [17], who effectively used an extremely large tensor strength (via a particular choice of parameter in the Δ propagator; see below), resulting in a very pronounced ''backward rise.'' A large tensor strength, very similar in magnitude to our fitted value C_t, has recently been found from a detailed analysis of the Δ resonance in the crossed reaction $\pi N\to\pi N$ [18,19]. Present quark-gluon models of the annihilation do not include sufficient correlations among the three quarks in the exchange channel to simulate a Δ propagation with the desired tensor strength. In our work we demonstrate that the two distinctive features visible in $p\bar{p}\to\pi^+\pi^-$, namely, the bump structure around 100° and the backward rise, can in fact be disentangled. The tensor meson f_2 causing the bump structure does not affect the backward angles; the ''backward rise'' is due to the Δ's tensor strength which, in turn, does not affect the bump structure. It is, of course, imperative to explain these two distinctive features at the quark-gluon (QCD) level. We will address this in a future communication. In the next section we describe the model (baryon-exchange plus meson pole diagrams) and derive the differential cross sections for $p\bar{p}\to\pi^+\pi^-$. The measured analyzing powers in this momentum range turn out to be dominated by the initial state interaction (ISI). If one wants to fine-tune the ISI, the comparison with the analyzing power will help to achieve this. In our analysis the ISI is important but not decisive for the understanding of the backward rise and the developing of the bump structure. We have, therefore, not attempted a comparison with the analyzing power. It should be noted here that our aim is *not* a least-χ^2 fit to the data but to point out the origin of the two main features of this reaction. There is certainly room for future improvement of the model. Section III contains our results and discusses the initial and finial state interactions. A detailed comparision with available data from CERN, KEK, and LEAR follows and the section ends with our conclusions.

II. BARYON-EXCHANGE PLUS MESON POLE MODEL

We start with the invariant scattering amplitude T for the reaction $NN\to\pi\pi$. The T is related to the standard S matrix with

$$S_{fi}=\delta_{fi}-\frac{i}{(2\pi)^2}\delta^{(4)}(P_f-P_i)\left(\frac{1}{2\omega_{k'}}\frac{1}{2\omega_k}\frac{M_N}{E_q}\frac{M_N}{E_{q'}}\right)^{1/2}T_{fi}, \tag{4}$$

where $q\equiv|\mathbf{q}|$, $k\equiv|\mathbf{k}|$, $q'\equiv|\mathbf{q}'|$, and $k'\equiv|\mathbf{k}'|$ with (see Fig. 1) $\mathbf{q}$, $\mathbf{q}'$, $\mathbf{k}$, and $\mathbf{k}'$ the momenta of the antiproton, proton, π^-, and π^+, respectively. $P_{f(i)}$ is the outgoing (incoming) total four-momentum, $E_q=\sqrt{\mathbf{q}^2+M_N^2}$, and $\omega_k=\sqrt{\mathbf{k}^2+m_\pi^2}$, with M_N (m_π) the nucleon (pion) mass.

The differential cross section of the process $\bar{N}N\to\pi\pi$ is given in the center-of-mass system

[1]For $P_{\rm lab}=500$ MeV/c experimental data yield the numbers $\sigma_{\rm tot}\approx 180$ mb, $\sigma_{\rm EL}\approx 60$ mb, $\sigma_{\rm CEX}\approx 14$ mb so that the annihilation cross section is $\sigma_{\rm ann}\equiv\sigma_{\rm tot}-\sigma_{\rm EL}-\sigma_{\rm CEX}\approx 106$ mb. On the other hand, $\sigma_{\pi\pi}\approx 0.4$ mb and $\sigma_{K\bar{K}}\approx 0.2$ mb so that $(\sigma_{\pi\pi}+\sigma_{K\bar{K}})/\sigma_{\rm ann}\approx 0.6\%$.

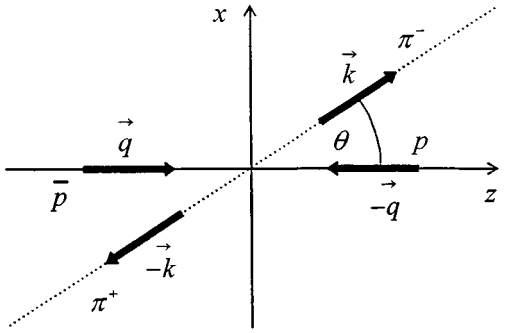

FIG. 1. Kinematics of the reaction $p\bar{p}\to\pi^+\pi^-$ in the c.m. system.

$$\frac{d\sigma_{\text{c.m.}}}{d\Omega}=\frac{1}{4(2\pi)^2}\frac{M_N^2}{(2E_N)^2}\frac{k}{q}|T|^2. \tag{5}$$

In the $|J,\lambda_1\lambda_2\rangle$ basis with J the total angular momentum and $\lambda_{1(2)}$ the proton (antiproton) helicity, $|T|^2$ is expressed as

$$|T|^2=\frac{1}{4}\sum_{\lambda_1\lambda_2}\sum_{JJ'}\frac{2J+1}{4\pi}\frac{2J'+1}{4\pi}(-1)^{\lambda}\langle k|T^J|q\lambda_1\lambda_2\rangle^*$$
$$\times\langle k|T^{J'}|q\lambda_1\lambda_2\rangle\sum_L C(JJ'L,\lambda-\lambda,0)P_L(\cos\theta), \tag{6}$$

where $\lambda=\lambda_1-\lambda_2$ and $\langle k|T^J|q,\lambda_1\lambda_2\rangle$ is the projection of the T matrix of the reaction $pp\to\pi^+\pi^-$ in the total angular momentum helicity basis. θ is the angle between $\mathbf{k}$ and $\mathbf{q}$, with choosing $\mathbf{q}$ along the z axis and $\mathbf{k}$ in the xz plane; see Fig. 1.

With the initial state interactions, one can express the T matrix of the reaction $p\bar{p}\to\pi^+\pi^-$ in the unitary form

$$\langle\pi^+\pi^-|T|N\bar{N}\rangle=\langle\pi^+\pi^-|W|N\bar{N}\rangle$$
$$+\langle\pi^+\pi^-|W|\alpha\rangle G\langle\alpha|T_{N\bar{N}}|N\bar{N}\rangle, \tag{7}$$

where $|\alpha\rangle$ can be any states allowed by conservation laws; see the previous section. We consider, in the present work, only $N\bar{N}$ intermediate states, namely, $|\alpha\rangle=|N\bar{N}\rangle$. For a discussion of the relative importance of other (mesonic) matrix elements see Ref. [17]. The first term in Eq. (7) corresponds to the processes illustrated in Figs. 2(a) and 2(b), and the second term to the processes in Figs. 2(c) and 2(d). The propagator G for the intermediate $N\bar{N}$ pair is defined as in the c.m. system,

$$G=\frac{1}{E-2E_p}, \tag{8}$$

with $E_p=\sqrt{\mathbf{p}^2+M_N^2}$ the energy of the intermediate nucleon. The T matrix of the reaction $p\bar{p}\to\pi^+\pi^-$ takes the form, in the angular momentum helicity state basis,

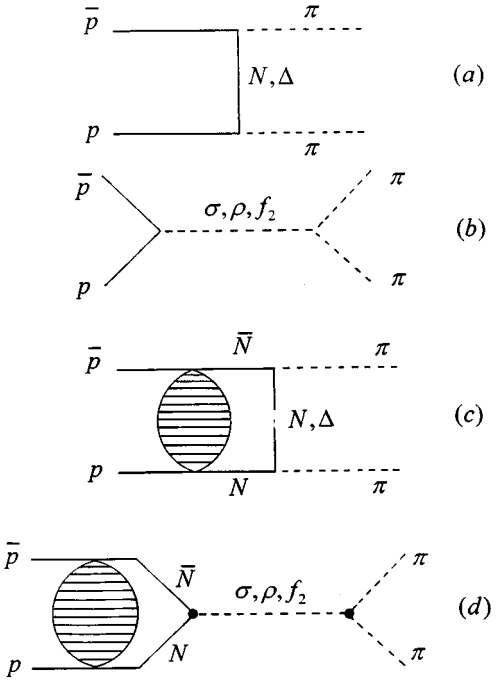

FIG. 2. Diagrams contributing to the reaction $p\bar{p}\to\pi^+\pi^-$. (a) and (c) the baryon-exchange process with N and Δ included, and (b) and (d) the process with mesons (σ, ρ, and f_2) as the intermediate state. The momentum of the intermediate N ($\bar{N}$) in (c) and (d) is $\mathbf{p}$ ($-\mathbf{p}$); see text. The solid circles in (d) represent the quark structure of these vertices; see text. The $T_{p\bar{p}\to N\bar{N}}$ as defined in Eq. (10) is denoted by the ellipses in (c) and (d).

$$\langle k|T^J|q,\lambda_1\lambda_2\rangle=\langle k|W^J|q,\lambda_1\lambda_2\rangle+\frac{1}{(2\pi)^3}\int_0^\infty p^2dp\frac{1}{E-2E_p}$$
$$\times\sum_{h_1h_2}\langle k|W^J|p,h_1h_2\rangle$$
$$\times\langle p,h_1h_2|T^J_{p\bar{p}\to N\bar{N}}|q,\lambda_1\lambda_2\rangle, \tag{9}$$

with

$$S_{p\bar{p}\to N\bar{N}}=\delta_{fi}-\frac{i}{(2\pi)^2}\delta^{(4)}(P_f-P_i)$$
$$\times\left(\frac{M_N}{E_p}\frac{M_N}{E_{p'}}\frac{M_N}{E_q}\frac{M_N}{E_{q'}}\right)^{1/2}T_{p\bar{p}\to N\bar{N}}, \tag{10}$$

where $\langle k|W^J|q,\lambda_1\lambda_2\rangle$ and $\langle p,h_1h_2|T^J|q,\lambda_1\lambda_2\rangle$ can be derived from the corresponding expressions in the helicity plane wave basis,

$$\langle p,h_1h_2|T^J|q,\lambda_1\lambda_2\rangle=2\pi\int_{-1}^{+1}dud^J_{\lambda h}(\theta)$$
$$\times\langle\mathbf{p},h_1h_2|T|\mathbf{q},\lambda_1\lambda_2\rangle, \tag{11}$$

$$\langle k|W^J|q,++\rangle=\int_{-1}^{+1}duP_J(u)\langle\mathbf{k}|W|\mathbf{q},++\rangle, \tag{12}$$

$$\langle k|W^J|q,+-\rangle=\int_{-1}^{+1}du\,\frac{[J(J+1)]^{1/2}}{2J+1}\,\frac{P_{J-1}(u)-P_{J+1}(u)}{\sin\theta}\times\langle\mathbf{k}|W|\mathbf{q},+-\rangle, \tag{13}$$

$$\langle k|W^J|q,++\rangle=\langle k|W^J|q,--\rangle, \tag{14}$$

$$\langle k|W^J|q,+-\rangle=\langle k|W^J|q,-+\rangle, \tag{15}$$

where $u=\cos\theta$, $\lambda=\lambda_1-\lambda_2$, $h=h_1-h_2$, and $\lambda_i=\pm\frac{1}{2}$ is denoted by $\pm$. $d^J_{\lambda h}$ are the reduced rotation matrices, $P_L(u)$ the Legendre polynomials.

Transforming the cross section in c.m. system to the laboratory frame, we have

$$\frac{d\sigma_{\rm lab}}{d\Omega}=t\frac{d\sigma_{\rm c.m.}}{d\Omega}, \tag{16}$$

with

$$t=\frac{[(g+\cos\theta)^2+(1-\beta^2)\sin^2\theta]^{3/2}}{(1-\beta^2)(1+g\,\cos\theta)}, \tag{17}$$

$$g=\beta\frac{E_\pi}{k}, \tag{18}$$

where β is the ratio of c.m. velocity to c and θ is the angle between the incoming $\bar{p}$ and outgoing π^- in the c.m. system; see Fig. 1.

A. Baryon-exchange diagrams

We consider first the exchange of the nucleon N in Fig. 2(a). The two $NN\pi$ vertex functions could be derived from the pseudovector Lagrangian

$$L_{NN\pi}=f_{NN\pi}/m_\pi\,\bar{N}\gamma^5\gamma^\mu\vec{\tau}N\cdot\partial_\mu\vec{\pi} \tag{19}$$

or from the pseudoscalar Lagrangian

$$L_{NN\pi}=g_{NN\pi}\,\bar{N}\gamma^5\vec{\tau}\cdot\vec{\pi}N. \tag{20}$$

However, our investigation shows that the coupling in Eq. (19) has a much better behavior than the one in Eq. (20) for high-energy $\bar{N}N\to\pi\pi$ processes if one has the half off-shell vertex functions [20], derived in the chirally symmetric quark model, to be used together with the above interactions. In the present work, we choose the interaction Lagrangian in Eq. (19) for a $NN\pi$ system, considering that the form is supported by the chiral quark model and matches the vertex functions mentioned above.

If a Δ is exchanged in Fig. 2(a), one will face a well-known problem. The Lagrangian describing a Rarita-Schwinger field is not unique. The kinetic term is of the general form [21]

$$L=\bar{\psi}^\alpha\Lambda_{\alpha\beta}\psi^\beta, \tag{21}$$

with

$$\Lambda_{\alpha\beta}=-[(-i\partial_\mu\gamma^\mu+M)g_{\alpha\beta}-iA(\gamma_\alpha\partial_\beta+\gamma_\beta\partial_\alpha)-iB\gamma_\alpha\gamma_\mu\partial^\mu\gamma_\beta-CM\gamma_\alpha\gamma_\beta], \tag{22}$$

where B and C are functions of the parameter A, $B=\frac{1}{2}(3A^2+2A+1)$ and $C=3A^2+3A+1$. The spin-$\frac{3}{2}$ propagator is dependent on A [21],

$$G_{\alpha\beta}(p)=\frac{i}{\gamma\cdot p-M}\left[g_{\alpha\beta}-\frac{1}{3}\gamma_\alpha\gamma_\beta-\frac{1}{3M}(\gamma_\alpha p_\beta-\gamma_\beta p_\alpha)-\frac{2}{3M^2}p_\alpha p_\beta\right]-\frac{1}{3M^2}\frac{A+1}{2A+1}\left[\gamma_\alpha p_\beta+\frac{A}{2A+1}\gamma_\beta p_\alpha+\left(\frac{1}{2}\frac{A+1}{2A+1}\gamma\cdot p-\frac{A}{2A+1}M\right)\gamma_\alpha\gamma_\beta\right]. \tag{23}$$

The physical properties of the free field are independent of the parameter A. In order that all physical observables involving an interacting $N\Delta\pi$ system be independent of A, the interaction Lagrangian must have the form

$$L_{N\Delta\pi}=\frac{f_{N\Delta\pi}}{m_\pi}\bar{\Delta}^\nu\mathbf{T}\theta_{\nu\mu}(X)N\partial^\mu\vec{\pi}+\text{H.c.}, \tag{24}$$

with

$$\theta_{\nu\mu}(X)=g_{\nu\mu}+\left[\frac{1}{2}(1+4X)A+X\right]\gamma_\nu\gamma_\mu, \tag{25}$$

$$\mathbf{T}=\left\{\begin{pmatrix}1&0\\0&\frac{1}{\sqrt{3}}\\-\frac{1}{\sqrt{3}}&0\\0&-1\end{pmatrix},\begin{pmatrix}-i&0\\0&-\frac{i}{\sqrt{3}}\\-\frac{i}{\sqrt{3}}&0\\0&-i\end{pmatrix},\begin{pmatrix}0&0\\\frac{2}{\sqrt{3}}&0\\0&-\frac{2}{\sqrt{3}}\\0&0\end{pmatrix}\right\}, \tag{26}$$

where H.c. stands for Hermitian conjugate and **T** is the isospin transition operator [22,23]. X is an arbitrary parameter. We choose $A=-1$ to simplify the propagator and adjust X to fit experimental data.

B. Meson-pole diagrams

Experiments have confirmed a number of mesons [13], which are strongly coupled to the $\pi^+\pi^-$ channel. Some of those mesons have the quantum numbers which a pair of NN could take, for instance, $\rho(770)$, $f_0(980)$, $f_0(1300)$, and $f_2(1270)$. Mesons above the NN threshold decaying into NN and $\pi^+\pi^-$ are, for example, $f_2(2150)$ and $\rho(2150)$. Therefore, one must include the pole diagram, namely, the process $p\bar{p}\to M(\text{meson})\to\pi^+\pi^-$ in the annihilation reaction of $p\bar{p}\to\pi^+\pi^-$. The investigations of the reaction $\pi N\to K\Sigma$ and $K\Lambda$ both in the effective $^3P_0$ quark model [24] and the resonance model [25] revealed that the two-step process is more important than the direct reaction.

The couplings of the scalar and vector mesons to the NN and $\pi\pi$ are widely studied. The interaction Lagrangians, for example, for the $NN\sigma$, $NN\rho$, $\pi\pi\sigma$, and $\pi\pi\rho$ systems are

$$L_{\sigma NN}=g_{\sigma NN}\bar{\psi}_N\psi_N\phi_\sigma, \tag{27}$$

$$L_{\rho NN}=g_{\rho NN}\bar{\psi}_N\gamma_\mu\vec{\tau}\cdot\vec{\phi}_\rho^{\,\mu}\psi_N+\frac{1}{4M_N}f_{\rho NN}\bar{\psi}_N\sigma_{\mu\nu}\times(\partial^\mu\vec{\phi}_\rho^{\,\nu}-\partial^\nu\vec{\phi}_\rho^{\,\mu})\cdot\vec{\tau}\psi_N, \tag{28}$$

$$L_{\sigma\pi\pi}=\frac{1}{2M_\pi}g_{\sigma\pi\pi}\phi_\sigma\partial_\mu\vec{\phi}_\pi\cdot\partial^\mu\vec{\phi}_\pi, \tag{29}$$

$$L_{\rho\pi\pi}=g_{\rho\pi\pi}(\vec{\phi}_\pi\times\partial_\mu\vec{\phi}_\pi)\cdot\vec{\phi}_\rho^{\,\mu}, \tag{30}$$

where $\sigma_{\mu\nu}=\frac{1}{2}[\gamma_\mu,\gamma_\nu]$ and ψ_N, ϕ_σ, and ϕ_ρ represent the nucleon, σ, and ρ fields, respectively.

Unlike the scalar and vector mesons, higher-spin meson fields cannot be uniquely described in the Lagrange formalism. And the evaluation of the pole diagram becomes more and more difficult as the spin of the intermediate meson increases. In addition to the scalar and vector mesons, we include here also the tensor meson, but not higher-spin states in the $p\bar{p}\to M\to\pi^+\pi^-$ process. There exits a free parameter in the Lagrangian describing a free tensor meson field, hence also in the propagator [26]. However, the physical properties of the field are independent of the free parameter appearing in the Lagrangian and propagator.

The couplings of the f_2 to the $\bar{N}N$ and $\pi\pi$ systems are described by the interaction Lagrangian [27]

$$L_{NNf_2}=i\frac{1}{2M_N}g_{NNf_2}(\bar{\psi}_N\gamma^\mu\partial^\nu\psi_N-\partial^\nu\bar{\psi}_N\gamma^\mu\psi_N)f_{\mu\nu}+\frac{1}{2M_N^2}f_{NNf_2}(\bar{\psi}_N\partial^\mu\partial^\nu\psi_N-\partial^\mu\bar{\psi}_N\partial^\nu\psi_N-\partial^\nu\bar{\psi}_N\partial^\mu\psi_N+\partial^\mu\partial^\nu\bar{\psi}_N\psi_N)f_{\mu\nu} \tag{31}$$

and

$$L_{\pi\pi f_2}=\frac{1}{2M_\pi}g_{\pi\pi f}(\vec{\phi}_\pi\partial^\mu\partial^\nu\vec{\phi}_\pi-\partial^\mu\vec{\phi}_\pi\partial^\nu\vec{\phi}_\pi)f_{\mu\nu}. \tag{32}$$

In the nonrelativistic limit, the first term on the right-hand side of Eq. (31) represents the f_2 coupling to the isoscalar NN state $^3P_2$ and the second to $^3F_2$. For the $\pi\pi f_2$ interaction, we include also the term $\vec{\pi}\partial^\mu\partial^\nu\vec{\pi}f_{\mu\nu}$. The interaction form in Eq. (32) ensures that the f_2 field couples to only the NN $J=2$ state. The second term in Eq. (32) represents the f_2 meson coupling to both the NN $J=0$ and $J=2$ states.

The propagators for the σ, ρ, and f_2 mesons are defined as

$$\Delta(p)=\frac{i}{p^2-M_\sigma^2}, \tag{33}$$

$$\Delta_{\mu\nu}(p)=\frac{-i}{p^2-M_\rho^2}(g_{\mu\nu}-p_\mu p_\nu/M_\rho^2), \tag{34}$$

$$\Delta_{\mu\nu\rho\lambda}(p)=\frac{i}{p^2-M_{f_2}^2}[g_{\mu\rho}g_{\nu\lambda}+g_{\mu\lambda}g_{\nu\rho}-\tfrac{2}{3}g_{\mu\nu}g_{\rho\lambda}+(g_{\mu\rho}p_\nu p_\lambda+g_{\mu\lambda}p_\nu p_\rho+g_{\nu\rho}p_\mu p_\lambda+g_{\nu\lambda}p_\mu p_\rho-\tfrac{3}{2}g_{\mu\nu}p_\rho p_\lambda-\tfrac{3}{2}g_{\rho\lambda}p_\mu p_\nu)/M_{f_2}^2+\tfrac{4}{3}p_\mu p_\nu p_\rho p_\lambda/M_{f_2}^4], \tag{35}$$

where the f_2 propagator in Eq. (35) is the form with[2] $A=-1$; see Ref. [26].

Since the propagator for a spin-2 meson involves a free parameter A [26], one will get contributions depending on it, according to the coupling of Eqs. (31) and (32). The contribution is off shell and only for the $J=0$ state. On the other hand, a coupling such as $\bar{\psi}_N g_{\mu\nu}\psi_N f_{\mu\nu}$ [not included in Eq. (31)] does not have on-shell contributions since the $f_{\mu\nu}$ field describing a spin-2 meson is traceless. However, such a term does contribute when the f_2 is off shell. This contribution is not to $J=2$, but to $J=0$ waves. These $J=0$ contributions are unphysical since the total angular momentum J (here the spin of intermediate mesons in the c.m. system) should be conserved in the process $p\bar{p}\to\pi^+\pi^-$. We employ the interaction Lagrangian in Eq. (31) for the NNf_2 coupling and let the parameter A in the propagator be -1 to avoid those unphysical contributions.

The transition amplitudes are worked out for the meson-pole diagrams mediated, respectively, by the scalar, vector, and tensor mesons as follows:

$$T_{p\bar{p}\to\sigma\to\pi^+\pi^-}(\lambda_1=1,\lambda_2=1)=g_\sigma\frac{q}{M_\pi M_N}\frac{E^2+k^2}{4E^2-M_\pi^2}, \tag{36}$$

$$T_{p\bar{p}\to\sigma\to\pi^+\pi^-}(\lambda_1=1,\lambda_2=-1)=0, \tag{37}$$

[2]The parameter A appearing in the general form of the f_2 propagator should not be confused with the parameter A appearing in Eqs. (23) and (25).

$$T_{p\bar{p}\to\rho\to\pi^+\pi^-}(\lambda_1=1,\lambda_2=1)=g_\rho\frac{k}{M_N W}\frac{W^2-q^2}{4E^2-M_\rho^2}\cos\theta - f_\rho\frac{kE}{M_N^2 W}\frac{W^2+q^2}{4E^2-M_\rho^2}\cos\theta, \tag{38}$$

$$T_{p\bar{p}\to\rho\to\pi^+\pi^-}(\lambda_1=1,\lambda_2=-1) = g_\rho\frac{k}{M_N W}\frac{W^2+q^2}{4E^2-M_\rho^2}\sin\theta - f_\rho\frac{kE}{M_N^2 W}\frac{W^2-q^2}{4E^2-M_\rho^2}\sin\theta, \tag{39}$$

$$T_{p\bar{p}\to f_2\to\pi^+\pi^-}(\lambda_1=1,\lambda_2=1) = g_{f_2}\frac{4qk^2}{3M_\pi M_N^2 W}\frac{q^2-W^2}{4E^2-M_{f_2}^2}P_2(\cos\theta) - f_{f_2}\frac{16q^3k^2}{3M_\pi M_N^3}\frac{1}{4E^2-M_{f_2}^2}P_2(\cos\theta), \tag{40}$$

$$T_{p\bar{p}\to f_2\to\pi^+\pi^-}(\lambda_1=1,\lambda_2=-1) = -g_{f_2}\frac{qk^2}{M_\pi M_N^2 W}\frac{W^2+q^2}{4E^2-M_{f_2}^2}\sin(2\theta), \tag{41}$$

with

$$g_\sigma=\frac{g_{NN\sigma}g_{\pi\pi\sigma}}{4\pi}, \tag{42}$$

$$g_\rho=\frac{g_{NN\rho}g_{\pi\pi\rho}}{4\pi}, \tag{43}$$

$$f_\rho=\frac{f_{NN\rho}g_{\pi\pi\rho}}{4\pi}, \tag{44}$$

$$g_{f_2}=\frac{g_{NNf_2}g_{\pi\pi f_2}}{4\pi}, \tag{45}$$

$$f_{f_2}=\frac{f_{NNf_2}g_{\pi\pi f_2}}{4\pi}, \tag{46}$$

where $E=\sqrt{q^2+M_N^2}$ and $W=E+M_N$. λ_1 and λ_2 represent the helicity of the initial proton and antiproton, respectively.

C. Initial state interactions and final state interactions

In principle, both the initial $N\bar{N}$ and final $\pi\pi$ interactions influence theoretical predictions. Although the final π's are quite relativistic in the process $p\bar{p}\to\pi^+\pi^-$, they are correlated in terms of the mesons discussed in Sec. II B, which form part of the FSI. This has been pointed out already in Ref. [28], which, however, does not include tensor mesons. Unlike the nucleon-nucleon force, the nucleon-antinucleon interaction is still not completely understood. Theoretical predictions are very model dependent, which directly influences the ISI. However, in the present work, fortunately, the ISI is not very important. Therefore we investigate only one version of the $N\bar{N}$ interaction to demonstrate the relative importance of the ISI. The initial state interaction is in the present work taken as the G-parity transformation of the energy-dependent one-boson-exchange Bonn potential (based on time-ordered perturbation theory, OBEPT) [22] plus an imaginary potential derived from a chiral quark model [8]. The imaginary optical potential is

$$\mathrm{Im}V_{\mathrm{opt}}(r)=W_0\rho^2(r), \tag{47}$$

where $\rho(r)$ is the $q\bar{q}$ annihilation density with r the relative distance of the N and $\bar{N}$ centers. The annihilation strength W_0 is treated as a free parameter and is found to be of order -1 to -2 GeV [8]. The form in Eq. (47) leads to a r-dependent range for the annihilation, unlike the exponential form used in Ref. [7] which has a range of 0.4 fm. Despite these differences the results obtained with Eq. (47) are very similar to the ones obtained with the one in Ref. [7].

III. RESULTS AND DISCUSSION

A. Predictions by the baryon-exchange diagrams

In this section we would like to show how much the exchange diagrams can contribute and how important the tensor coupling of the $N\Delta\pi$ system is. As usual, vertex functions appear due to the quark substructure of hadrons. The coupling constants are related to $g_{N\bar{N}\pi}$ with the following relations as derived in chiral quark models [20,23]:

$$f_{NN\pi}^2=(m_\pi/2M_N)^2 g_{NN\pi}^2,\quad f_{N\bar{N}\pi}^2=(m_\pi/2M_N)^2 g_{N\bar{N}\pi}^2,$$
$$f_{N\Delta\pi}^2=\tfrac{72}{25}f_{NN\pi}^2,\quad f_{\bar{N}\Delta\pi}^2=\tfrac{72}{25}f_{N\bar{N}\pi}^2,$$
$$g_{N\bar{N}\pi}=\tfrac{1}{13}g_{NN\pi},\quad \frac{g_{NN\pi}^2}{4\pi}=14.4. \tag{48}$$

The half off-shell vertex functions employed here are those from Ref. [20]. Those vertex functions depend on the quark energy E_0 and on the cutoffs $\Lambda_k(N)$, $\Lambda_k(\Delta)$, $\Lambda_E(N)$, and $\Lambda_E(\Delta)$. The center-of-mass corrected quark eigenenergy E_0 is $\frac{1}{2}M_N$ [20]; the cutoffs Λ are partially taken from form factor data [29] and partially fitted to $pp\to\pi^+\pi^-$. We find that the data prefer

$$\Lambda_k(N)=\Lambda_k(\Delta), \tag{49}$$

$$\Lambda_E(N)=\Lambda_E(\Delta). \tag{50}$$

We find from a comparison with data that the energy cutoff Λ_E, Eq. (50), cannot be smaller than the three-momentum cutoff Λ_k, Eq. (49), if Λ is in the region 0.5−2.0 GeV. Otherwise, predictions for the differential cross section will be much larger than experimental data if one still uses the coupling constants mentioned above. The Λ_E should be always larger than Λ_k, $\delta=\Lambda_E-\Lambda_k=0.1-0.3$ GeV, depending slightly on the value of Λ_k; see Table I.

In addition to the cutoffs Λ, C_t is also adjusted to experiments. We find that an energy-dependent C_t describes

TABLE I. Parameters used in the baryon-exchange process in Fig. 2(a). The second and third lines are, respectively, for the models with and without the $N\Delta\pi$ tensor coupling.

Λ_k (GeV)	Λ_E (GeV)	C_0	C_1 (GeV^{-1})	C_2 (GeV^{-2})
1.04	1.17	-0.50	-0.47	0.43
0.60	0.82	0.0	0.0	0.0

present data better than a constant C_t. The energy dependence of C_t could be described as

$$C_t = C_0 + C_1 * q + C_2 * q^2, \tag{51}$$

where C_0, C_1, and C_2 are free parameters and $q \equiv |\mathbf{q}|$, with $\mathbf{q}$ as defined in Fig. 1.

The results for the baryon-exchange diagrams alone [i.e., Fig. 2(a)] are presented in Fig. 3. The parameters are given in Table I.

We find, in Fig. 3, that the observed backward enhancement of differential cross sections cannot be understood in a baryon-exchange model without the $N\Delta\pi$ tensor coupling. This confirms the findings of Ref. [17]. The baryon-exchange model with a suitable $N\Delta\pi$ coupling supports a reasonably good fit to differential cross sections for low-energy $pp \to \pi^+\pi^-$ reactions and gives a considerable backward enhancement. The magnitude of the $N\Delta\pi$ tensor coupling C_0 is very similar to the value in the crossed reactions [18,19]. The baryon exchange model of Refs. [7,28] does not include the $N\Delta\pi$ tensor coupling and, hence, considerably underestimates the backward cross section of $p\bar{p} \to \pi^+\pi^-$. This latter feature is not improved by adding the FSI [28]; see Sec. II C.

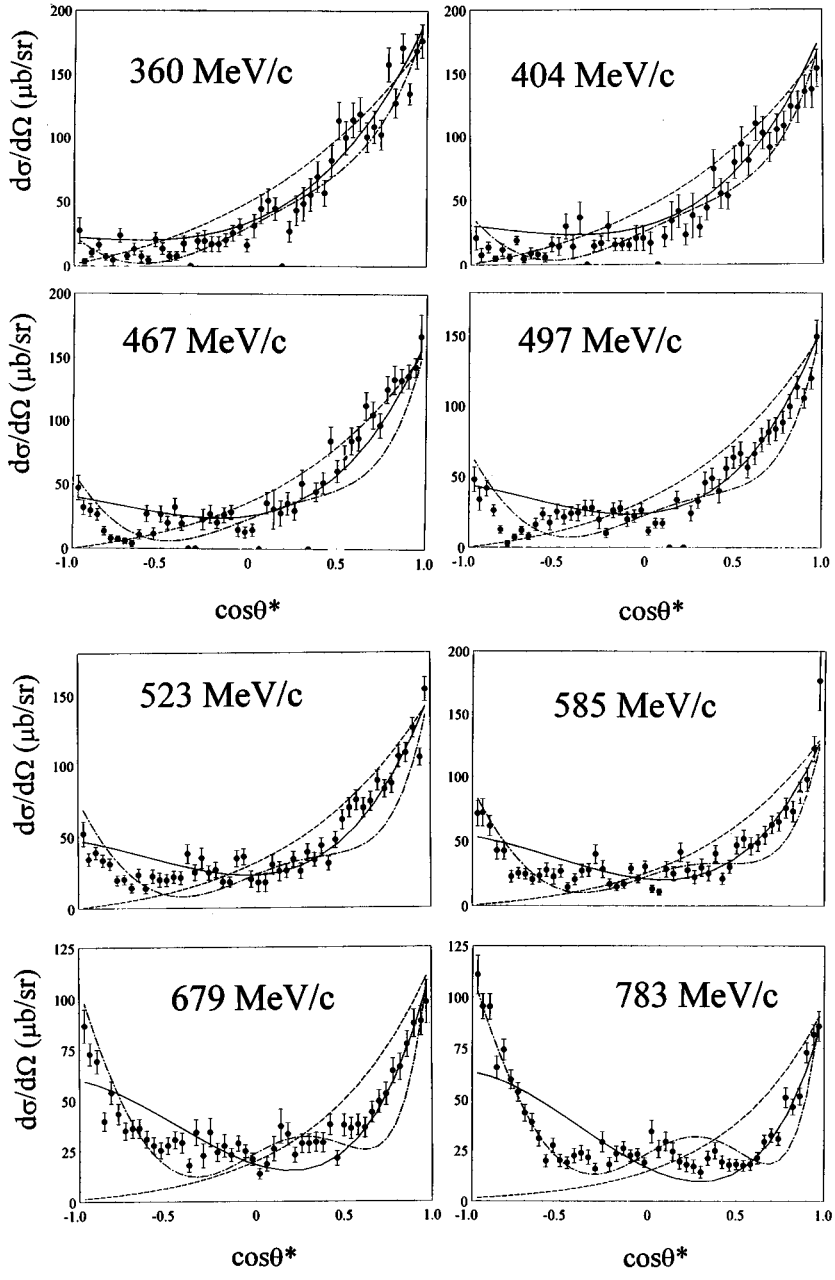

FIG. 3. Predictions for differential cross sections in the baryon-exchange diagrams alone and in the model involving both the baryon-exchange and meson-pole diagrams. The solid and dashed lines refer to the baryon-exchange models with and without the $N\Delta\pi$ tensor coupling, respectively. The dash-dotted lines are the predictions of the full model. The experimental data are from Ref. [12].

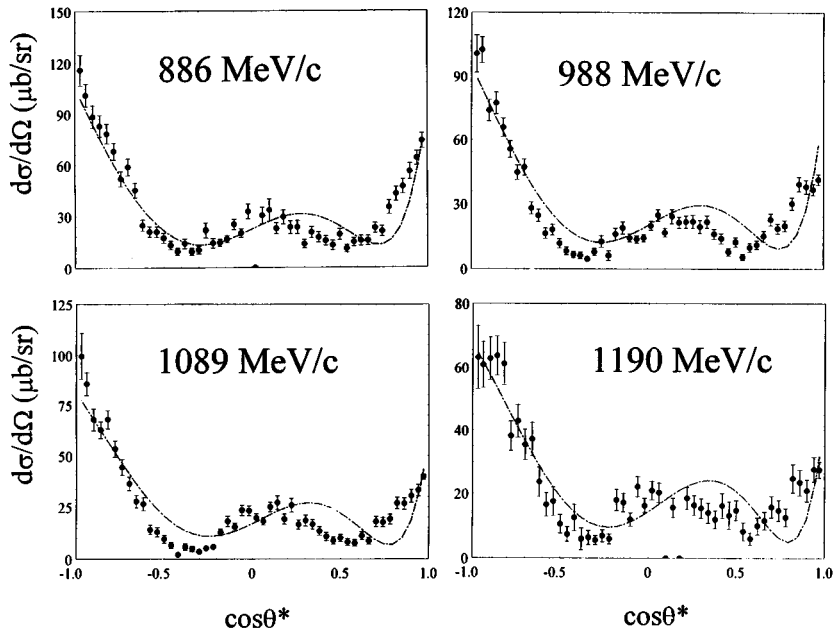

FIG. 3. (*Continued*)

The model of Ref. [17] does not *explictly* introduce a $N\Delta\pi$ tensor coupling, but it is equivalent to a baryon-exchange model with $A=-1$ and $C_t=-1$. Although the model of Ref. [17] confirms the findings $C_t\neq 0$ and negative, such extremely large $|C_t|$ is neither supported by our analysis nor by the analysis of [18,19]. It has also been found that C_t should take negative values [18,19] by an investigation of the crossed reaction of pion-nucleon scattering. We find $C_t=-1/2$ in the present work when the initial proton is at rest, which implies equal strength for scalar and tensor couplings in the $N\Delta\pi$ system. The field theory of supersymmetry and supergravity [30] also supports $C_t=-\frac{1}{2}$.

The baryon-exchange model considered here with a nonvanishing $N\Delta\pi$ tensor coupling contributes sizably to the backward differential cross section of $p\bar{p}\to\pi^+\pi^-$. But it fails to reproduce the bump structure at the scattering angle of about 100° for higher energies. In the following, we show that the problem can be solved by including meson-pole diagrams.

B. Predictions with both the baryon-exchange and meson-pole diagrams

In this subsection, we add meson-pole diagrams to baryon-exchange diagrams discussed previously. Like the baryon-exchange process, coupling constants and vertex functions are needed for the vertices MNN and $M\pi\pi$ in the reaction $p\bar{p}\to M(\text{meson})\to\pi^+\pi^-$. However, there are no reliable coupling constants and vertex functions; the choice by the authors is quite different.

Vertex functions used for the exchange diagram cannot be used for the pole diagram since the three-momentum of the intermediate meson vanishes for the process $p\bar{p}\to M\to\pi\pi$ in the center-of-mass system. In fact, we have little knowledge on timelike vertex functions for the pole diagram. We try to derive our vertex functions from quark models. Based upon the predictions of amplitudes for the processes of $NN\to M\to M_1M_2$ in the present Lagrangian approach and the $^3P_0$ nonrelativistic quark model [31,32], one could extract the forms of the MNN and $M\pi\pi$ vertex functions. The vertex functions are derived as follows for the $M\pi\pi$ and MNN couplings:

$$F_{M\pi\pi}(k)=\exp(-\alpha k^2), \tag{52}$$

$$F_{MN\bar{N}}(p)=\exp(-\beta q^2), \tag{53}$$

where $q=|\mathbf{q}|$ and $k=|\mathbf{k}|$; see Fig. 1. Because of the relation $\mathbf{k}^2+m_\pi^2=\mathbf{q}^2+M_N^2$, the two functions in Eqs. (52) and (53) are not independent for unconstrained coupling constants. According to the $^3P_0$ quark model, $\alpha\approx 2\beta$. In the present work, we set $\alpha=2\beta$ and adjust the parameter β to experimental data.

The amplitudes in Eqs. (36)–(41) depend only mildly on the mass of the intermediate meson,

$$\frac{1}{4E-M}, \tag{54}$$

resulting from the propagators. In the present work $M_\sigma=650$ MeV, $M_\rho=770$ MeV, and $M_{f_2}=1270$ MeV. The ρ and f_2 mesons are the lowest-mass vector and tensor mesons decaying into $\pi\pi$ and $\pi\pi/KK$, respectively [13]. The σ meson mass parametrizes the FSI in the isoscalar-scalar $\pi\pi$ channel, in accordance with Refs. [22,33]. As for the mass distribution of the mesons, we just replace the masses above with complex masses involving widths such as $M=M_0+i\Gamma/2$. We use[3] [13] $\Gamma_\rho=150$ MeV, $\Gamma_\sigma=300$ MeV, and $\Gamma_{f_2}=180$ MeV. According to our investigation, the mass distributions effect final results very little, so that their contributions could be safely neglected.

[3]The decay width of the fictitious σ meson is taken according to Ref. [33].

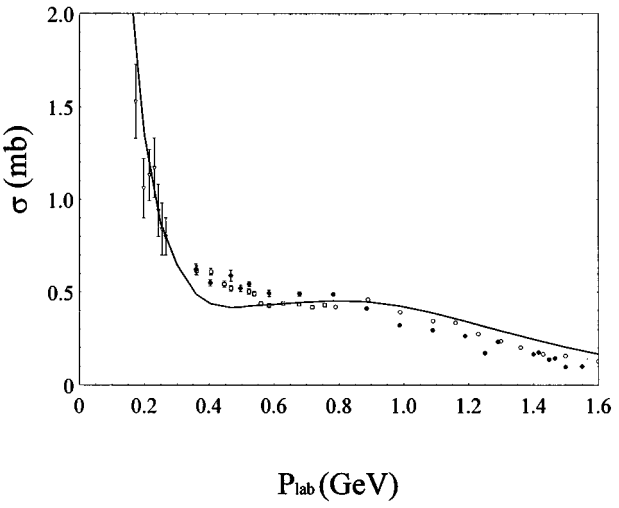

FIG. 4. Prediction for the integrated cross section as a function of $P_{\rm lab}$. Experimental data from Refs. [12] (solid circles, LEAR), [35] (circles, CERN), [36] (squares, KEK), and [37] (triangles, LEAR).

We present, in Fig. 3 and Fig. 4, the theoretical predictions with both the baryon-exchange diagrams and the meson-pole diagrams mediated by the scalar, vector, and tensor mesons. The integrated cross sections are well reproduced for $P_{\rm lab}=200-1600$ MeV/c. The plateau between 500 and 800 MeV is also present in our model. The differential cross sections display the main features (backward enhancement for all energies, bump structure for higher energies) fairly well. The relevant parameters are collected in Table II. The values of parameters in the left and right columns are, respectively, for the cases without and with initial state interactions.

We find in Table II that the cutoff Λ_k here is very close to the prediction in a chiral quark model [20,29], where Λ_k is derived from a comparison to axial vector form factor data [29]. We find $\Lambda_E \approx \Lambda_k$ within $\sim 10\%$, which confirms the findings of Ref. [20]. This energy ''smearing'' was introduced in Ref. [20] to account for center-of-mass effects in the energy of the bound three-quark system. There is a substantial energy exchange between quarks so that their actual energy can deviate quite a bit from the single-quark eigenenergy $E_0=\frac{1}{2}M_N$. The energy transfer from the quarks and antiquarks bound in N and $\bar{N}$ to the quarks and antiquarks bound in $\pi^{\pm}$ is substantial and necessitates such an energy smearing of bound quarks and antiquarks in hadrons.

TABLE II. Parameters adjusted to experimental data in the model including both the baryon-exchange and meson-pole diagrams. The second column is for the process without the ISI shown in Figs. 2(a) and 2(b), the third for the full model denoted by all the diagrams in Fig. 2.

Λ_k (GeV)	0.77	0.76
Λ_E (GeV)	0.87	0.86
C_0	-0.50	-0.50
C_1 (GeV^{-1})	-0.58	-0.55
C_2 (GeV^{-2})	0.48	0.44
β (GeV^{-2})	2.75	2.70
g_{f_2}	0.17	0.16
f_{f_2}	1.23	1.17
g_ρ	0.36	-0.49
f_ρ	0.36	-0.56
g_σ	0.85	0.89

The tensor strength parameter C_0 is very close to other findings [18,19,30], while the energy dependence parameters $C_{1,2}$ represent our prediction. Our values for β and α defined in Eqs. (52) and (53) correspond to a size parameter 0.8 fm for the MNN vertex and 1.1 fm for the $M\pi\pi$ vertex. Note that these values cannot directly be compared with size parameters obtained for spacelike form factors, like $G_{\pi NN}(q^2)$. Our values indicate that the annihilation $N\bar{N}\to M$ occurs in a smaller region than the hadronization process $M\to\pi\pi$ requires. This is reminiscent of the old ''fireball'' picture for the annihilation process, where the fireball expands before hadronizing into light mesons. It should also be noted here that the absolute values of the size parameters are averaged values for $M=\sigma,\rho,f_2$ with very different masses involved. The coupling constants in Table II are the values with the initial nucleon (antinucleon) at rest and the final pions on shell, so that they are related to timelike vertex functions and not to spacelike form factors and coupling constants as reported in [19,33,34]. Spacelike and timelike vertex functions have to be related via analytic continuation, resulting in quite different values, for example, for $g_{\pi NN}$ and $g_{\pi N\bar{N}}$; see Eq. (48) and Ref. [20]. We find that our timelike coupling constants g_ρ, f_ρ, and g_σ are smaller than the spacelike values reported in [19,33,34].

The coupling constants g_σ, g_{f_2}, and f_{f_2} are stable with respect to variations of the initial state interaction and with respect to different weights attributed to different scattering angles (for example, the backward or the forward direction) or with respect to the selected momentum range (for example, the lowest energies or the higher-momentum range of the old CERN data). According to the $^3P_0$ nonrelativistic quark model, the coupling constants g_{f_2} should be larger than the f_{f_2} in the concerned energy range if the intermediate f_2 in the process $p\bar{p}\to M(\text{meson})\to\pi^+\pi^-$ is a pure $q\bar{q}$ state [31]. But in the present work we find that f_{f_2} is much larger than g_{f_2}. This suggests that there exist strong correlations among pure $q\bar{q}$ states and gluon-rich states with the f_2 quantum numbers in the process $p\bar{p}\to f_2\to\pi^+\pi^-$. Unlike the g_σ, g_{f_2}, and f_{f_2}, the g_ρ and f_ρ are very sensitive to the initial state interaction and the automatic fitting process. Quite different magnitudes, even different signs, can be obtained when one uses different initial state interactions or different distributions of fitting weights. However, the ratio of the f_ρ to g_ρ is always around 1.0 when the f_ρ and g_ρ vary. This ratio is smaller than the corresponding spacelike values. Finally it should be pointed out that the coupling constants shown in Table II should be seen to parametrize the scalar-isoscalar, vector-isovector, and tensor-isoscalar strength in both the $\pi\pi$ and $N\bar{N}$ channels, without reference to specific resonances, like $\rho(770)$, ρ', ρ'', $f_2(1270)$, $f_2(1225)$, $f_2(2150)$, etc.

We summarize several points here.

(1) In the theoretical predictions in Figs. 3 and 4, the baryon-exchange diagrams are dominant for reactions with

the lowest momenta. As the incoming momentum is increased, the meson-pole diagrams become more and more important. The backward enhancement is mostly contributed by the tensor coupling of the $N\Delta\pi$ system while the bump structure for higher momenta is mainly due to the tensor meson-pole diagram, although all the scalar, vector, and tensor meson-pole diagrams are necessary to reproduce the observed bump structure.

(2) Without the process $p\bar{p}\rightarrow f_2\rightarrow\pi^+\pi^-$, one could also get a small bump structure for higher-momentum reactions although at too large an angle. It will be interesting to see how spin-3 and spin-4 mesons contribute in the $\theta\approx 100°$ region [14].

(3) The ISI diagrams in Figs. 2(c) and 2(d) contribute about 20% to the final results. However, after refitting free parameters to experimental data, one gets almost the same prediction for both with and without the initial state interaction. We conclude from this that the two dominant features of this reaction (backward enhancement and bump structure above 670 MeV/c) cannot be attributed to the ISI.

Our analysis of hadronic diagrams, supplemented with subhadronic QCD vertex functions, identifies the main ''problem areas'' of quark-gluon models in this reaction: The exchanged three-quark system has to be correlated such that a strong $N\Delta\pi$ tensor coupling results. In the direct channel the gluonic intermediate states GGG, $GG\bar{q}q$, and $Gq^2\bar{q}^2$ must be correlated to form a significant tensor meson strength in the mass region $1.2-2.0$ GeV. Both features represent a formidable challenge for nonperturbative quark-gluon models. Work along these lines is in progress.

[1] G. Baur *et al.*, Phys. Lett. B **368**, 251 (1996).

[2] C. Amsler and F. Myhrer, Annu. Rev. Nucl. Part. Sci. **41**, 219 (1991); R. Armenteros and B. French, *High Energy Physics* (Academic Press, London, 1969), Vol. 4, p. 237.

[3] E. Eisenhandler *et al.*, Phys. Lett. **47B**, 531 (1973); Nucl. Phys. **B113**, 1 (1976); J. Sedlak and V. Simak, Sov. J. Part. Nucl. **19**, 191 (1988).

[4] L. Michel, Nuovo Cimento **10**, 319 (1953); D. Amati and B. Vitale, *ibid.* **2**, 719 (1955); C. Goebel, Phys. Rev. **103**, 258 (1956); T.D. Lee and C.N. Yang, Nuovo Cimento **3**, 749 (1956); L. Wolfenstein, Phys. Rev. **135**, B1436 (1964).

[5] R. Tegen, in *Proceedings of the 1987 Cape Town Workshop on Quarks, Gluons and Hadronic Matter*, edited by R. D. Viollier and N. Warner (World Scientific, Singapore, 1987), p. 354.

[6] T.E.O. Ericson and F. Myhrer, Phys. Lett. **74B**, 163 (1978).

[7] T. Hippchen *et al.*, Phys. Rev. C **44**, 1323 (1990); V. Mull *et al.*, *ibid.* **44**, 1337 (1990); V. Mull and K. Holinde, *ibid.* **51**, 2360 (1995).

[8] F. Myhrer and R. Tegen, Phys. Lett. **162B**, 237 (1985).

[9] R. Tegen, T. Mizutani, and F. Myhrer, Phys. Rev. D **32**, 1672 (1985).

[10] R. Tegen, F. Myhrer, and T. Mizutani, Phys. Lett. B **182**, 6 (1986).

[11] S. Kahana *et al.*, Phys. Rev. C **28**, 1393 (1983).

[12] A. Hasan *et al.*, Nucl. Phys. **B378**, 3 (1992).

[13] Particle Data Group, Phys. Rev. D **50**, 1173 (1994).

[14] W.M. Kloet and F. Myhrer, Phys. Rev. D **53**, 6120 (1996).

[15] V. Mull and K. Holinde (private communications).

[16] H. Genz, Phys. Rev. D **31**, 1136 (1985); M. Kohno and W. Weise, Nucl. Phys. **A454**, 429 (1986); M. Maruyama and T. Ueda, *ibid.* **A364**, 297 (1981); Phys. Lett. B **124**, 121 (1983); M. Maruyama, Prog. Theor. Phys. **69**, 937 (1983); C.B. Dover and P.M. Fishbone, Nucl. Phys. **B244**, 349 (1984); A.M. Green *et al.*, Phys. Lett. **121B**, 101 (1983); A.M. Green and J. Niskanen, Nucl. Phys. **A412**, 448 (1984); R.A. Freedman, W.Y.P. Hwang and L. Wilets, Phys. Rev. D **23**, 1103 (1981); M.A. Alberg *et al.*, *ibid.* **27**, 536 (1983); A. Faessler *et al.*, *ibid.* **26**, 1663 (1985); S. Furui and A. Faessler, Nucl. Phys. **A424**, 525 (1984); M. Maruyama, S. Furui, and A. Faessler, *ibid.* **A472**, 643 (1987); M. Maruyama, S. Furui, A. Faessler, and R. Vinh Mau, *ibid.* **A473**, 649 (1987); T. Gutsche, M. Maruyama, and A. Faessler, *ibid.* **A503**, 737 (1989); C.B. Dover, T. Gutsche, M. Maruyama, and A. Faessler, Prog. Part. Nucl. Phys. **29**, 87 (1992); T. Gutsche, R.D. Viollier, and A. Faessler, Phys. Lett. B **331**, 8 (1994); R. Tierauf, T. Gutsche, Y. Yan, A. Muhm, and A. Faessler, Nucl. Phys. **A588**, 783 (1995); A.M. Green and J.A. Niskanen, in *International Review of Nuclear Physics*, edited by T.T.S. Kuo (World Scientific, Singapore, 1984) Vol. 1, p. 569; U. Hartmann, E. Klempt, and J.G. Körner, Phys. Lett. **155B**, 163 (1985).

[17] B. Moussallam, Nucl. Phys. **A429**, 429 (1984).

[18] A. Schmidt, M.Sc. thesis, University München, 1994; see also V. Bernard *et al.*, Z. Phys. A **348**, 317 (1994).

[19] B.C. Pearce and B.K. Jennings, Nucl. Phys. **A528**, 655 (1991).

[20] J. Speth and R. Tegen, Nucl. Phys. **A511**, 716 (1990).

[21] M. Benmerrouche *et al.*, Phys. Rev. C **39**, 2339 (1988).

[22] R. Machleidt, K. Holinde, and Ch. Elster, Phys. Rep. **149**, 1 (1987).

[23] G.E. Brown and W. Weise, Phys. Rep. C **22**, 281 (1975).

[24] Y. Yan, S.W. Huang, and A. Faessler, Phys. Lett. B **354**, 24 (1995).

[25] K. Tsushima, S.W. Huang, and A. Faessler, Phys. Lett. B **337**, 245 (1994).

[26] L.M. Nath, Nucl. Phys. **68**, 660 (1965).

[27] M. Suzuki, Phys. Rev. D **47**, 1043 (1992); and (private communication).

[28] V. Mull *et al.*, Phys. Lett. B **275**, 12 (1992).

[29] R. Tegen and W. Weise, Z. Phys. A **314**, 357 (1983).

[30] P. Van Nieuwenhuizen, Phys. Rep. **68**, 189 (1981).

[31] Y. Yan, Ph.D thesis, Universität Tübingen, 1994.

[32] A. Le Yaouanc, L. Oliver, Opène, and J.-C. Raynal, Phys. Rev. D **8**, 2223 (1972).

[33] C. Schütz, J.W. Durso, K. Holinde, and J. Speth, Phys. Rev. C **49**, 2671 (1993).

[34] C. Lee, S.N. Yang, and T.-S.H. Lee, J. Phys. G **17**, L131 (1991).

[35] E. Eisenhandler *et al.*, Nucl. Phys. **B96**, 109 (1975).

[36] T. Tanimori *et al.*, Phys. Rev. D **41**, 744 (1990).

[37] G. Bardin *et al.*, Phys. Lett. B **192**, 471 (1987).